DEM modelling and analysis of the mixing characteristics of sphere-cylinder granular mixture in a rotating drum

Jiang, Chuanning; An, Xizhong; Li, Meng; Wu, Yuhang; Gou, Dazhao; Wu, Yongli

DOI
10.1016/j.powtec.2023.118653

Publication date
2023

Document Version
Final published version

Published in
Powder Technology

Powder Technology 426 (2023) 118653

Contents lists available at ScienceDirect

Powder Technology

journal homepage: www.journals.elsevier.com/powder-technology

DEM modelling and analysis of the mixing characteristics of sphere-cylinder granular mixture in a rotating drum

Chuanning Jiang [a], Xizhong An [a,*], Meng Li [a], Yuhang Wu [a], Dazhao Gou [b], Yongli Wu [c]

[a] *Key Laboratory for Ecological Metallurgy of Multimetallic Mineral of Ministry of Education, School of Metallurgy, Northeastern University, Shenyang 110819, PR China*
[b] *School of Materials Science and Engineering, University of New South Wales, Sydney 2052, Australia*
[c] *Section of Resource and Recycling, Faculty of Civil Engineering & Geosciences, Delft University of Technology 2628, CN, Delft, the Netherlands*

HIGHLIGHTS

- Mixing of different binary spheres/cylinders mixtures was numerically reproduced.
- Effects of operation conditions and materials properties on mixing were investigated.
- Various macro/micro properties during mixing were quantitatively characterized.
- The underlying mechanisms were explored through energy analysis of different zones.

GRAPHICAL ABSTRACT

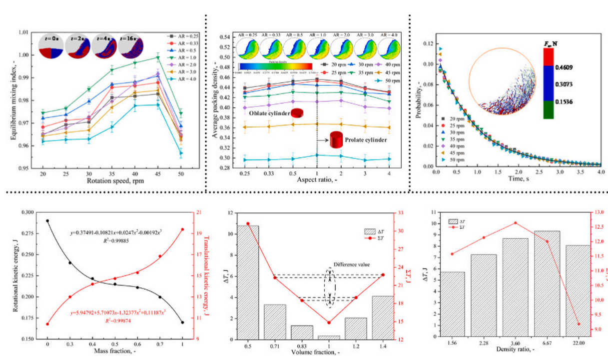

ARTICLE INFO

Keywords:
Mixing
Spheres/cylinders binary mixtures
Numerical simulations
Mechanisms

ABSTRACT

Mixing structures and characteristics are crucial to the mixing quality of spherical/cylindrical binary granular systems like the biomass-coal mixtures which can affect energy release and carbon emissions. In this work, the mixing of binary spheres/cylinders in a rotating drum was numerically reproduced by using discrete element method (DEM). Systematic parametric studies were conducted to identify the role of various parameters such as rotation speed (ω) of the drum, aspect ratio (AR), mass fraction (φ_c) and volume fraction (φ_v) of cylindrical particles, and the density difference (φ_ρ) between the binary particles; meanwhile, corresponding mechanisms were also explored by analyzing the kinetic energy. Results show that when the flow regime is rolling/cascading, the mixing quality can be effectively improved; however, when the flow regime is cataracting, the mixing quality becomes worse. With AR close to 1.0, the interlocking effect between particles becomes weaker and the porosity becomes smaller, which leads to the higher contact efficiency and thus improves the mixing quality. Binary mixtures with different φ_c are synergistically affected by energy input and interlocking structure. The volume of spherical particles is more conducive to improving the mixing quality than that of cylindrical particles when the volume of the granular system is at the same level. The φ_ρ can cause segregation behavior of particles so as to make the mixing quality worse.

* Corresponding author.
E-mail address: anxz@mail.neu.edu.cn (X. An).

https://doi.org/10.1016/j.powtec.2023.118653
Received 28 March 2023; Received in revised form 5 May 2023; Accepted 11 May 2023
Available online 12 May 2023
0032-5910/

1. Introduction

Granular matter is widely used in industrial areas such as chemical engineering, pharmaceutical industry, food industry, and so on [1]. Due to the influence of material physical properties (e.g., particle density, size and shape) and operating conditions (e.g., rotation speed), granular matter in a rotating drum exhibits complex flow behavior and mixing characteristics. At present, the flow pattern (i.e., slipping, slumping, rolling, cascading, cataracting and centrifuging) of granular matter in a rotating drum has been successfully analyzed [2]. However, how to obtain those high-quality mixtures (e.g., spherical/cylindrical binary mixtures) with optimized structures and utilization efficiencies is still people's main concern and yet to be properly solved.

In order to identify the mixing characteristics and flow behaviors of granular matter in a rotating drum, different experimental approaches have been developed and utilized in the past decades. For example, for complicated three-dimensional systems, the probe method and the freeze-cutting method can be used to investigate the overall mixing of particles in a rotating drum. Although these methods are effective in characterization, they are destructive to the structure [3]. Tomography, velocity measurement and spectroscopy can characterize and evaluate the flow and mixing behavior of particles in a rotating drum without destroying the granular system [4–10], while these methods are really difficult to visualize and quantify the motion behavior of internal particles in the mixing process. In addition, the mixing behaviors are also closely related to the micromechanical properties (e.g., inter-particle interaction forces) of the system, which are hard to be monitored or characterized in-situ in physical experiments.

In comparison, numerical modelling has become an important alternative to experiments in conveniently and cost-effectively investigating the multiscale properties of particulate systems. In particular, the discrete element method (DEM) has been demonstrated as a powerful tool in identifying the particle scale dynamics (e.g., flow, structures, and forces) of various granular systems during mixing in rotating drums. At present, based on DEM simulations, researchers have systematically explored the effects of particulate properties like particle size [11], density [12], Young's modulus [13], friction coefficient [14–16] on the mixing behaviors of spheres. In addition, the effects of drum geometry [17–21] and the operation parameters like rotation speed [22], filling fraction [23–25] and movement mode [26] of the drum on the mixing behaviors of spheres have also been well studied. Fortunately, different methods for characterizing particle shapes have been developed in recent years, which led many researchers to shift their interest in the mixing of particulate matter from spheres to non-spherical particles. As a kind of representative non-spherical particles, the mixtures of cylindrical particles have attracted researchers' attention due to their applications in chemical and energy industries (e.g., plastics and biomass) [7,27]. In this aspect, Kodam et al. [28] analyzed the contact position and detection between two cylinders, and reproduced the movement behavior of cylinder mixtures in the drum by using the multi-sphere model. Zhao et al. [29] studied the effect of shape index on the accurate description of the sharpness of the cylinder edges by using super-ellipsoid model. Ma et al. [30] explored the positional relationship between cylindrical particles and the end plate of the drum during mixing process. Yang et al. [31,32] simulated the effects of aspect ratio (AR) on the flow characteristics and length ratio between different cylindrical particles on the flow behavior and dynamics in the drum in rolling regime.

The maturity of methods for characterizing particle shape makes the mixing process of multi-shape particles become a reality. As a representative mixture of multi-shape particles, sphere-cylinder granular matter has attracted much attention due to its important applications in industry (e.g., fuel blends of biomass and coal materials) [33,34]. Although a large amount of numerical work was carried out in the past decades, there are few studies on the mixing of sphere-cylinder granular mixtures in a rotating drum [35]. Therefore, the focus of our work was to further explore the optimal operation/material parameters in achieving a desired mixing of such a binary mixture, the evolution of macroscopic mixing behaviors and its underlying mechanisms related to the microscopic particle scale structures and dynamics, which can guide for better industrial applications.

In this work, DEM is used to numerically study the mixing process and flow behaviors of different binary sphere-cylinder particulate systems in a rotating drum. At a macroscopic scale, the effects of the critical parameters (i.e., rotation speed of the drum (ω), aspect ratio (AR), mass fraction (φ_c) and volume fraction (φ_v) of cylindrical particles, and density difference (φ_ρ)) on the mixing characteristics are systematically investigated; on this basis, the correlation between mixing quality and operation parameters was established. At a microscopic scale, the particle scale properties (e.g., contact force and force structures, particle orientation, and kinetic energy) are characterized and analyzed, and then the underlying mechanisms were characterized through energy analysis of different zones (e.g., spheres; cylinders) in binary system.

2. Numerical method and simulation conditions

2.1. Particle shape model

In previous simulations, different methods which include the super-ellipsoid model [30], the polyhedron model [36], and the multi-sphere model [37] were used by different researchers to describe the shapes of the involved non-spherical particles. By comprehensive consideration of the computational efficiency and accuracy, the super-ellipsoid model was utilized to construct cylindrical particles in the current work. The

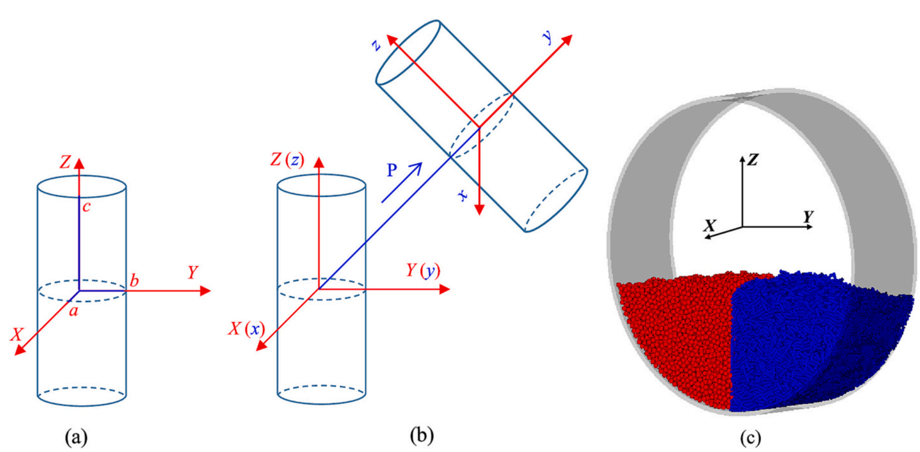

Fig. 1. Coordinate systems used in the simulations, where: (a) the coordinate system with the origin coinciding with the centroid of the cylinder; (b) the coordinate system with the movement of the cylinder; (c) schematic of the utilized horizontal rotating drum, in which the two end planes of the drum are not shown.

simulations were conducted by using the commercial DEMSlab V5.0 software. Here, the standard super-ellipsoid model is defined as [30,38]:

$$f(x,y,z) = \left(\left|\frac{x}{a}\right|^{s_2} + \left|\frac{y}{b}\right|^{s_2}\right)^{\frac{s_1}{s_2}} + \left|\frac{z}{c}\right|^{s_1} - 1 = 0 \quad (1)$$

where a, b, c are three semi-major axes of a particle; s_1 and s_2 are the shape indexes to describe the edge sharpness of particles, where $s_1 = 20$ and $s_2 = 2$ are set to ensure both the sufficient accuracy and the computation efficiency. The shape parameter is defined as AR $= a/c$. Cylinders are prolate when $c \geq a = b$ and oblate when $c < a = b$. In the simulations, ARs ranging from 0.25 to 4.0 are utilized to characterize shapes from oblate to prolate cylinders as shown in Fig. A1 in ***Appendix A***, where $d_v = 12$ mm refers to the diameter of a sphere with equivalent volume of a cylinder.

It needs to note that Eq. (1) can be used only when the center and the three major axes of the cylindrical particle coincide with the coordinate origin and the three coordinate axes, respectively. When the cylindrical particle is at the optional position in the global coordinate system X-Y-Z, the local coordinate system x-y-z needs to be introduced, with the coordinate origin and coordinate axes coinciding with the particle centroid and the axes of the particle, respectively, as shown by Fig. 1(a). However, the position relationship between the cylindrical particle and the coordinate system of the solved space generally does not meet the above conditions in practical application. As shown in Fig. 1(b), for describing each cylindrical particle, it is necessary to perform the coordinate transformation by a matrix, $\boldsymbol{B}$, as indicated by:

$$X = \boldsymbol{B}x + P \quad (2)$$

here, $\boldsymbol{B}$ can be expressed as:

$$\boldsymbol{B} = \begin{bmatrix} cos\lambda cos\mu - sin\lambda cos\sigma sin\mu & -cos\lambda sin\mu - sin\lambda cos\sigma cos\mu & sin\lambda sin\sigma \\ sin\lambda cos\mu + cos\lambda cos\sigma sin\mu & -sin\lambda sin\mu + cos\lambda cos\sigma cos\mu & -cos\lambda sin\sigma \\ sin\sigma sin\mu & sin\sigma cos\mu & cos\sigma \end{bmatrix} \quad (3)$$

in which $x = (x, y, z)^T$ and $X = (X, Y, Z)^T$ are position vectors in the local and global coordinate systems, respectively; $P = (x_0, y_0, z_0)^T$ is the position vector of the particle centroid in the global coordinate system; and (λ, σ, μ) are Euler angles [30]. In addition, the utilized horizontal rotating drum before mixing is schematically shown in Fig. 1(c).

2.2. Governing equations

In the DEM model, the translational motion and rotational motion of each particle can be governed by Newton's second law as:

$$m_p \frac{d\boldsymbol{v}_p}{dt} = \boldsymbol{F}_p + m_p\mathbf{g} \quad (4)$$

$$\boldsymbol{I}_p \frac{d\boldsymbol{w}_p}{dt} = \boldsymbol{T}_p \quad (5)$$

where m_p, $\boldsymbol{v}_p$, $\boldsymbol{I}_p$, $\boldsymbol{\omega}_p$ and $\mathbf{g}$ are the mass, translational velocity, inertia moment, angular velocity, and gravity acceleration of particle p, respectively; $\boldsymbol{F}_p$ and $\boldsymbol{T}_p$ are the contact force and contact torque acting on particle p. The contact force of each particle can be calculated using a standard soft sphere linear spring-dashpot model [39]. Particle orientation is a significant parameter in determining both the rotation and the contact status of non-spherical particles. It needs to specify that similar approach as that in Refs. [30, 40, 41] was used to characterize interparticle contacts.

2.3. Simulation conditions

The simulation parameters are selected with reference to biomass and coal. It should be noted that the component of biomass has large effects on the density [42–46]. Similarly, coal has different densities due to its different mineral compositions [47–51]. Coincidentally, the densities between long flame coal [47] and biomass [52] (e.g., sugarcane bagasse, maize stalk, etc.) are similar. Therefore, the influence of ω and AR on mixing was studied in the premise of ensuring the same density. Other parameters (φ_c, φ_v, and φ_ρ) were explored on the basis of the aforementioned preferred mixtures. Here, the sliding and rolling friction coefficients between particles and between particles and the walls of the drum are selected by Refs. [37, 53]. In addition, the DEM time step was set to 1×10^{-5} s to ensure the stability of the numerical simulation, which was equivalent to 15% of the Rayleigh time [37,52]. The total number of spherical and cylindrical particles is 22,000, where the details of model validation and simulation parameters are given in ***Appendix B*** and Table 1, respectively.

Table 1
Process parameters used in the simulations.

Parameters	Values
Drum diameter, D (mm)	700
Drum length, L (mm)	240
Cylinder length, l (mm)	2.0801–13.2077
Cylinder diameter, d (mm)	3.3020–8.3204
Sphere diameter, d_s (mm)	12
Aspect ratio, AR	0.25–4.0
Particle density, ρ (kg/m^3)	1200
Young's modulus, Y (N/m^2)	2.6e+10
Poisson's ration, ν	0.29
Restitution coefficient between particles, e	0.5
Sliding friction coefficient between particles, μ_s	0.4
Rolling friction coefficient between particles, μ_r	0.005
Restitution coefficient between particle and wall, e_1	0.5
Sliding friction coefficient between particle and end wall, μ_{s1}	0.05
Rolling friction coefficient between particle and end wall, μ_{r1}	0.005
Sliding friction coefficient between particle and curved wall, μ_{s2}	0.5
Rolling friction coefficient between particle and curved wall, μ_{r2}	0.005
Number of particles, N	22,000
Filling level δ	39.7855%–42.3570%
Rotation speed, ω (rpm)	20–50
Simulation time, T (s)	30
Mesh size, d_c (mm)	$3d_v \times 3d_v \times 3d_v$
Time step, Δt (s)	1.00e-05

3. Results and discussion

3.1. The influences of rotation speed on mixing

The instantaneous mixing quality is proposed to quantify the mixing process. In current work, the evolution of the Lacey mixing index is fitted by the error function [54]:

$$M(t) = M_0 + (M_f - M_0)erf(Rt) \quad (6)$$

where M_0 and M_f are respectively initial and final mixing indexes. R represents the mixing rate. For details, please refer to ***Appendix C***. It is necessary to point out that the mixing quality is better when the mixing index is close to 1.0. Besides, the characterization of the Lacey mixing index is affected by the division of grid cells. So the rotating drum is divided into several cubes with equal size in this study, where the side length of each cube is set to 3 times the equivalent diameter of particles d_v, which was verified by the grid independence in previous studies [37,55]. Fig. 2(a) gives the temporal evolution of mixing patterns of spheres (red)/cylinders (blue) mixture at different ω. As can be seen that during mixing the spiral band between spheres and cylinders gradually blurs due to their mutual diffusion in the radial direction. After sufficient time, spherical and cylindrical particles are randomly and uniformly distributed in the rotating drum to form the final steady state. It is also interesting to note that the spiral band disappears faster at 40 rpm and 50 rpm, which means that increasing ω is conducive to improving the

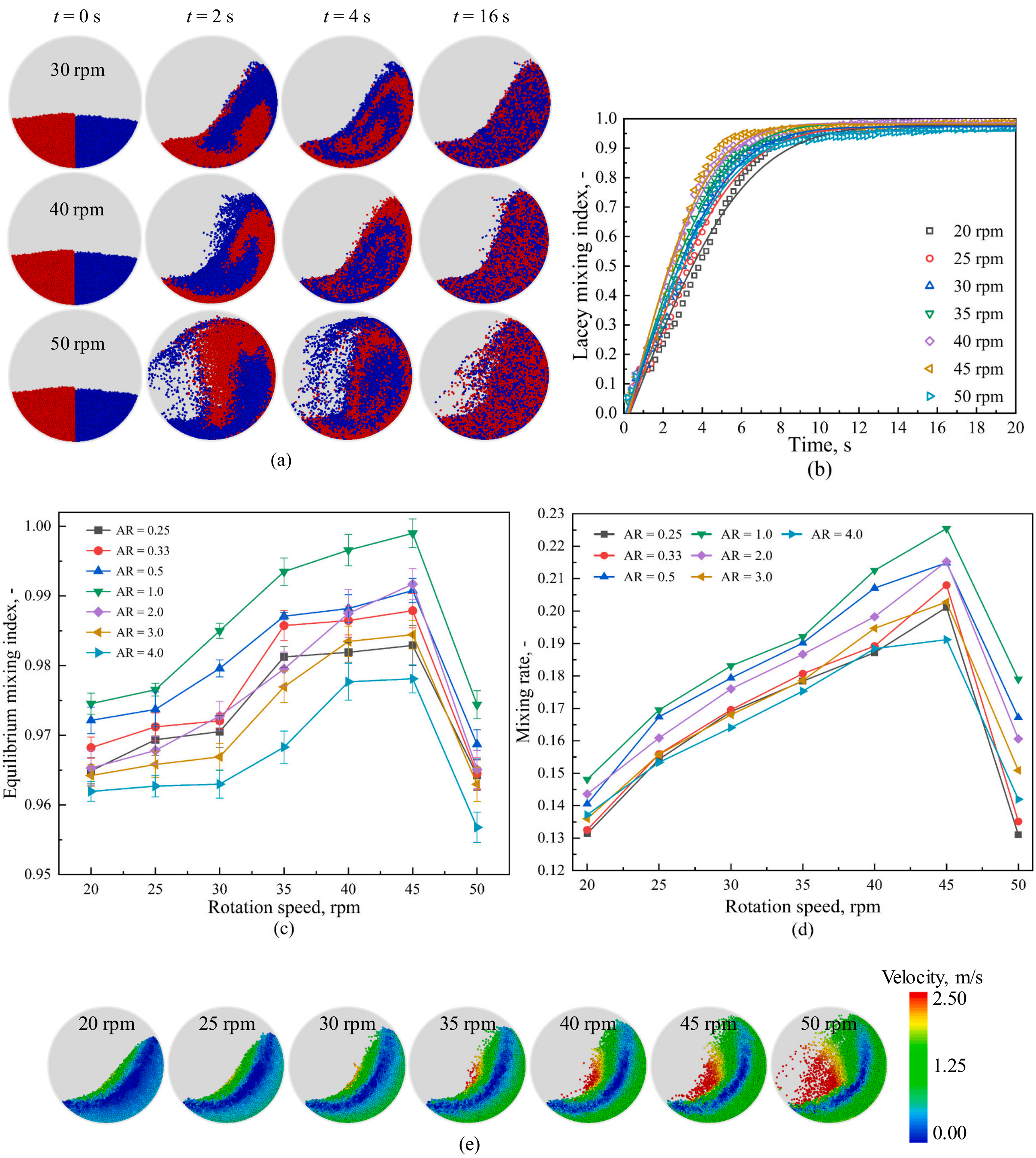

Fig. 2. (a) Temporal evolution of mixing patterns of spheres (red)/cylinders (blue, AR = 1.0) mixture at different ω; (b) Lacey mixing index as a function of time at different ω for the mixtures with AR = 1.0; evolution of the equilibrium mixing index (c) and mixing rate (d) for each binary mixture under different ω; (e) the velocity profiles of the mixtures with AR = 1.0 in the drum under different ω. (For interpretation of the references to colour in this figure legend, the reader is referred to the web version of this article.)

mixing quality. Fig. 2(b) shows the evolution of the Lacey mixing index at different ω for the mixture with AR = 1.0, where the solid lines represent the fitting results according to the Eq. 6. For details of other conditions, please refer to ***Appendix D***. To describe the mixing quality more accurately, the influences of ω on the equilibrium mixing index and mixing rate of binary mixtures were discussed. To reduce the error to the minimum, the equilibrium mixing index is averaged in each case at 3 different time steps after the granular system in the drum reaches a steady state. The mixing quality and mixing rate of each mixture are better at 45 rpm as shown in Fig. 2(c) and (d). As shown in Fig. 2(e), this is mainly due to the fact that the flow regime of the granular bed behaves in rolling/cascading flow regime at 20–45 rpm. With the increase of ω from 45 rpm to 50 rpm, the flow regime turns into cataracting and the time to achieve a well-mixed state becomes longer, which is consistent with the phenomenon found by Gui et al. [24,56].

In addition to the uniformity, the packing density, defined as the volume ratio of particles versus the whole granular bed, has a significant effect on the heat and mass transfer within a packed bed. To reduce the error, we choose three different time steps to average the local packing density when the granular system reaches a stable state. The inset figure in Fig. 3 shows that with the increase of ω, the local packing densities of passive layer (rubbing against the wall of the rotating drum) and static layer (middle) are reduced, and the packing density of the granular system tends to be uniform [14]. Furthermore, the effects of ω on the

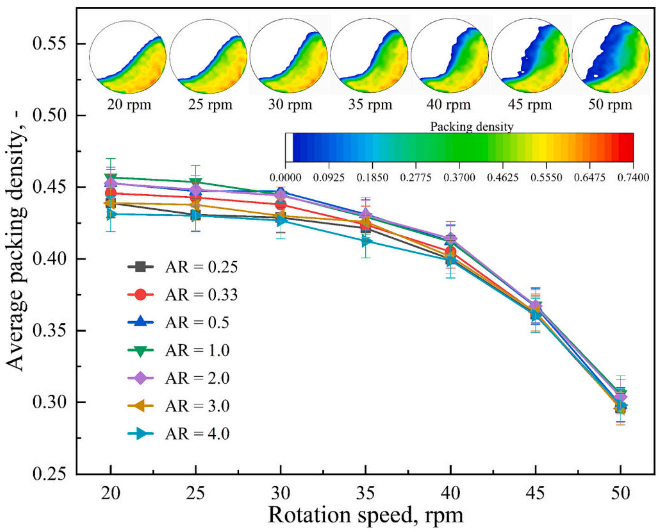

Fig. 3. Evolution of average packing density of each binary mixture as a function of ω, where the inset figures show binary mixtures with AR = 1.0 under different ω.

average packing density are quantitatively analyzed. Fig. 3 indicates that the average packing density of the binary system gradually decreases with the increase of ω, which provides a basis for the packing density of the static and passive layers of the granular system to become uniform at a higher ω. Additionally, it needs to specify that the bed starts to expand as ω increases. In conclusion, for each binary mixture, increasing ω can decrease the average packing density and loosen the packing structure due to the expansion of the granular bed. It is of great significance to study the heat transfer or drying behavior of the drum.

As the main way to transfer energy, the interaction between particles and the inner walls of the drum can directly affect the mixing quality. It is known that any system obeys the law of energy conservation, and the binary system is no exception. Particles in the free layer (rolling or falling on the surface of the granular bed) are driven by gravity and friction to roll or slide. The static layer is driven by the inter-particle friction. In the passive layer, the particle movement is mainly driven by the friction of p-p (particle-particle) and p-w (particle-wall). It is widely known that the energy of the granular system is mainly formed by particles in the passive layer, that is to say, the fundamental reason for the energy of the granular system is the work done by friction. However, the magnitude and direction of the inter-particle friction are changing all the time, which brings great difficulties to research. In fact, the work by the friction of the granular system can be given according to the law of energy conservation, which can effectively simplify the problem. For the binary system, the energy conservation can be expressed as:

$$W_k + W_g + Q = W_f \quad (7)$$

where W_k, W_g and W_f are the kinetic energy, gravity potential energy and friction work of the granular system (energy input), and Q is the energy dissipated by friction or collision. Fig. 4(a) shows that the kinetic energy of the granular system increases with ω. And the difference of the translational/rotational kinetic energy between particles first increases and then decreases, which means the velocity difference is maximum at 45 rpm. In order to describe the height of the granular system more simply, the position of the gravity center of the granular bed is given in Fig. 4(b). It indicates that with the increase of ω, the gravity center of the granular bed gradually increases, implying that the granular system has greater gravitational potential energy. In addition, it has been proven that the frequency of inter-particle collisions increases with ω [14,37]. In other words, with the increase of ω from 20 rpm to 45 rpm (rolling/cascading regime), the friction of the granular system is dominant and the position of particles in the drum is effectively increased, which leads to the increase of the velocity difference between particles and thus promotes the mixing process. When ω is increasing from 45 rpm to 50 rpm, the translation of flow regime from rolling/cascading to cataracting results in the decrease of the velocity difference, which increases the particle trajectory and decreases the probability of convective diffusion between spherical particles and cylindrical particles. It also proves that the cataracting regime is inferior to the flow regime of rolling/cascading in the mixing process [57].

3.2. The influences of AR on mixing

Particle shape is the essential factor affecting the mixing characteristics. Fig. 5(a) shows that for each ω, the peak of the equilibrium mixing index-AR curve always appeared at AR = 1.0. Interestingly, the similar trend appears on the mixing rate-AR curve, as shown in Fig. 5(b). It means that a cylindrical particle without prominent length in both the axial and radial direction is conducive to improving the mixing quality of binary mixtures. In view of the above trend, we analyzed the influence of AR on

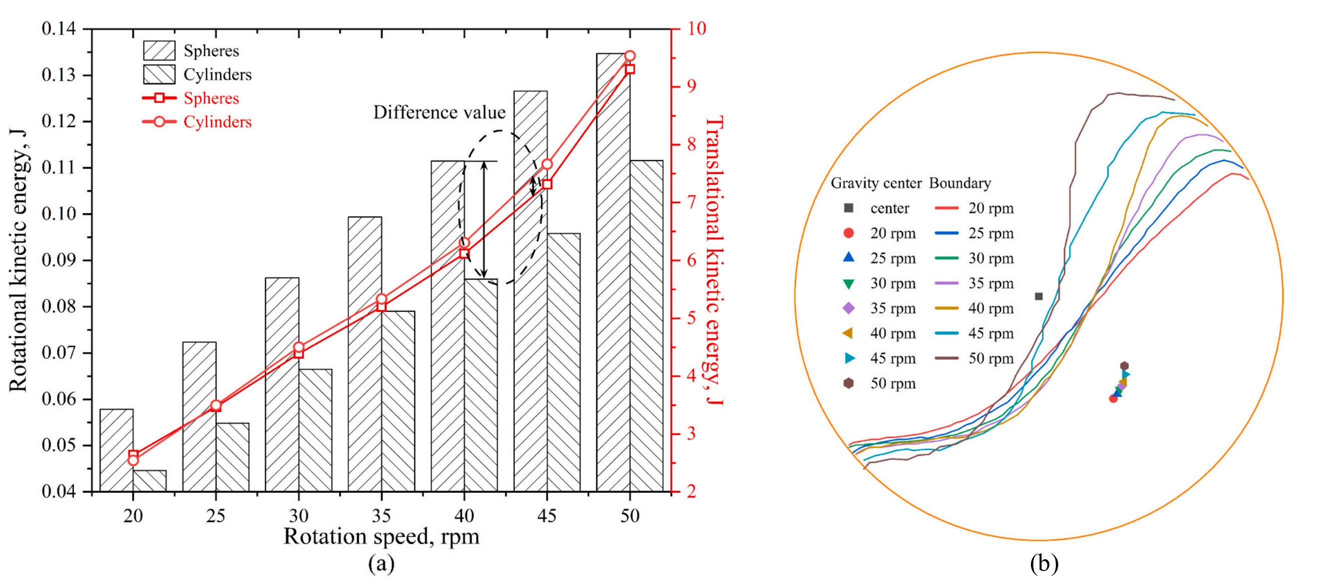

Fig. 4. (a) Evolutions of the rotational and translational kinetic energy within different zones as a function of rotation speeds when AR = 1.0; (b) the gravity center of the granular bed with different ω when AR = 1.0.

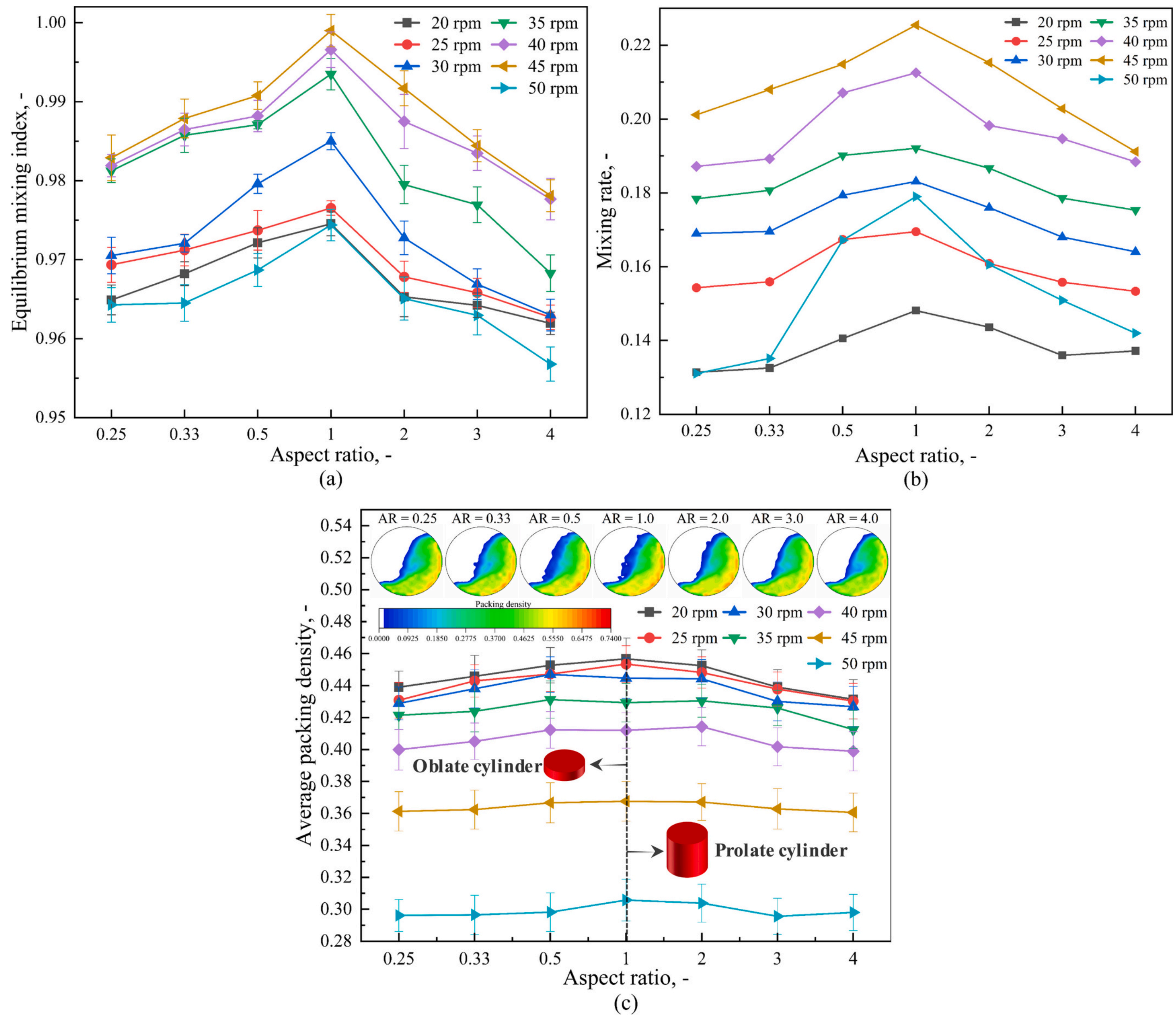

Fig. 5. Evolution of the equilibrium mixing index (a) and mixing rate (b) for each binary mixture under different ARs; evolution of average packing density of each binary mixture as a function of AR, where the inset figures show binary mixtures with different ARs at 45 rpm.

the average packing density. Fig. 5(c) shows that the average packing density is larger as AR is close to 1.0. Combined with the inset in Fig. 5(c), it can be found that with AR close to 1.0, the average packing density is smaller in the free layer, while that in the passive layer is opposite. It can be inferred that pores in the passive layer of binary mixtures with AR close to 1.0 are effectively filled, which can promote energy input of the granular system and the energy transfer of p-p and p-w.

The forces acted on particles are the key factor in determining the flow behavior, structure and properties of binary mixtures. In the mixing process, the particle movement in a rotating drum is driven by centripetal force, which is very complicated and can be indicated by the interaction of various forces like gravity, radial centrifugal force, friction and normal force of p-p and p-w. It can be observed from Fig. 6(a) that larger normal contact forces are mainly distributed in the middle and tail parts of the granular bed [37]. The larger normal contact force at the tail part of the granular bed is caused by the falling impact of particles and the normal force between particles, while the larger normal contact force in the middle part of the granular bed is assigned to the normal force between particles and the particle-wall friction. For more quantitative analysis, probability distributions of normal contact forces under different ω and ARs are investigated. For more concise and much clearer analysis, the forces are normalized by its average value and gravity, respectively. The results in Fig. 6(b) indicate that ω has no obvious effect on the normal contact force, while the probability of smaller normal contact forces increases as AR deviates from 1.0. Meanwhile, the inset figure of Fig. 6(c) also shows that ω has no significant effect on the force distribution. In order to clearly observe the effect of AR on the normal contact force, the Gaussian distribution is fitted to the values under different conditions, in which the fitting confidence of each function is $\geq$ 97.29%. The fitted data have been given in Fig. 6(c), where both θ and δ firstly decrease and then increase. And both θ and δ become the smallest when AR = 1.0, which indicates that the normal contact force in the mixture with AR = 1.0 is the largest and best concentrated. Therefore, it can be estimated that there are more frequent contacts and the high efficiency of force transfer in the mixture with AR = 1.0.

As one of the inherent characteristics of cylinders, the particle orientation is an important parameter that has a significant influence on the mixing behavior and structure of the granular system. For more quantitative analysis, Euler angles (λ, σ, μ) under different ARs are investigated when the granular system reaches a stable state. The ranges of λ, σ, and μ

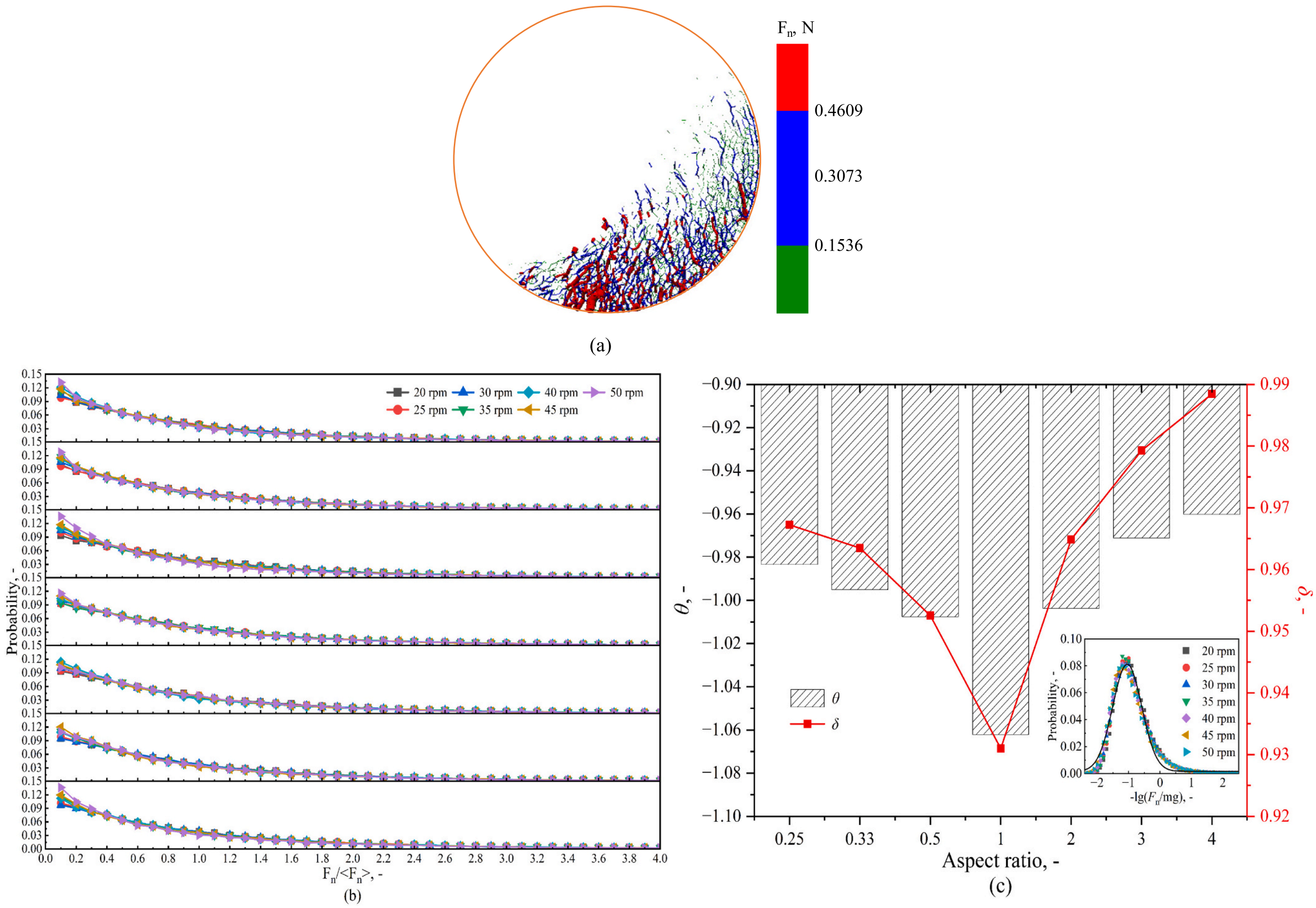

Fig. 6. (a) Spatial distributions of normal contact forces in the binary mixture with AR = 1.0 at 45 rpm; (b) probability distributions of normal contact force in binary mixtures under different conditions; (c) fitting of mean value (θ) and standard deviation (δ) of each mixture with Gaussian distribution, where the inset figure shows probability distributions of logarithmic normal contact force in binary mixtures with AR = 1.0 under different rotation speeds.

are $[-\pi, \pi]$, $[0, \pi]$, $[-\pi, \pi]$, respectively. Here, the ranges of λ and μ are equivalently adjusted to $[0, \pi]$. In order to clearly observe the change of the particle orientation, we normalize the λ, σ and μ with π to obtain the ternary distribution diagram of particle orientation when the ω is 45 rpm. Fig. 7(a-d) indicates that as AR < 1.0, the orientation distribution in the dotted line area shows an increasing trend along the *M* direction (λ and σ decrease; μ increases), which means that the radial direction of oblate cylinders tends to parallel to the rotation direction. In contrast, Fig. 7(d-g) demonstrates that the orientation distribution in the dotted line area shows an increasing trend along the *N* direction (λ and μ increase; σ decreases) when AR > 1.0, which implies that the major axis of the prolate cylinders inclines to be parallel to the rotation direction. The trend when AR > 1.0 is consistent with the one reported by Ma et al. [30]. In conclusion, on one hand, oblate/prolate cylindrical particles are in a structure conducive to the mixing process because of the effect of convection between particles; on the other hand, due to the friction between particles and between particles and drum walls, the structure is in a relatively stable state.

As is well known that the mixing process between particles is caused by convection and diffusion [58]. Convection is induced by the velocity difference between particles in the granular bed. Particles will diffuse from one side to the other when convection occurs. In order to better understand the effect of AR on diffusion, the average velocities of different zones (e.g., spheres; cylinders) were analyzed when the granular system reaches a stable state. To reduce the error, we choose five different time steps to average the velocity. Fig. 8 shows that the average velocity of spheres is slightly higher than that of cylinders at 20 rpm (rolling). It is because binary mixtures have the larger average packing density and smaller pores at low rotational speed, which makes the interlocking structure between particles more stable and restricts the motion of cylinders with obvious radial and axial length. However, with the increase of ω from 25 rpm to 45 rpm (cascading), the average velocity of cylinders with AR = 0.25, AR = 0.33, AR = 3.0, AR = 4.0 is lower than that of spheres. It is because the expansion of the granular bed results in the decrease of the average packing density and the increase of pores (the interlocking is destroyed to a certain extent), which promotes the motion of spheres and cylinders. Compared to spheres, the motion of cylinders is weaker due to the obvious radial and axial length. In contrast, cylinders (AR = 0.5, AR = 1.0, AR = 2.0) without apparent radial and axial length are easier to move than spheres as ω increases from 25 rpm to 45 rpm. When ω continues increasing to 50 rpm (cataracting), the granular bed expands violently and the constraints between particles are extremely reduced. Cylindrical particles dominate the mixing process at this stage. There is no doubt that it leads to the lower final mixing quality due to the overactive behavior of the granular bed which weakens the diffusion behavior between particles. To sum up, spheres play a major role in diffusion at low rotational speed (rolling). Cylinders with AR = 0.5, AR = 1.0 and AR = 2.0 play a major role in diffusion at relatively high rotational speed (cascading); spheres play a major role in diffusion at relatively high rotational speed when AR is 0.25, 0.33, 3.0, 4.0. Cylinders play a major role in diffusion at high rotational speed (cataracting).

3.3. *The influences of mass fraction on mixing*

Mass fraction is also a critical influencing factor for the mixing process of the binary system. To explore the mass faction effects, the

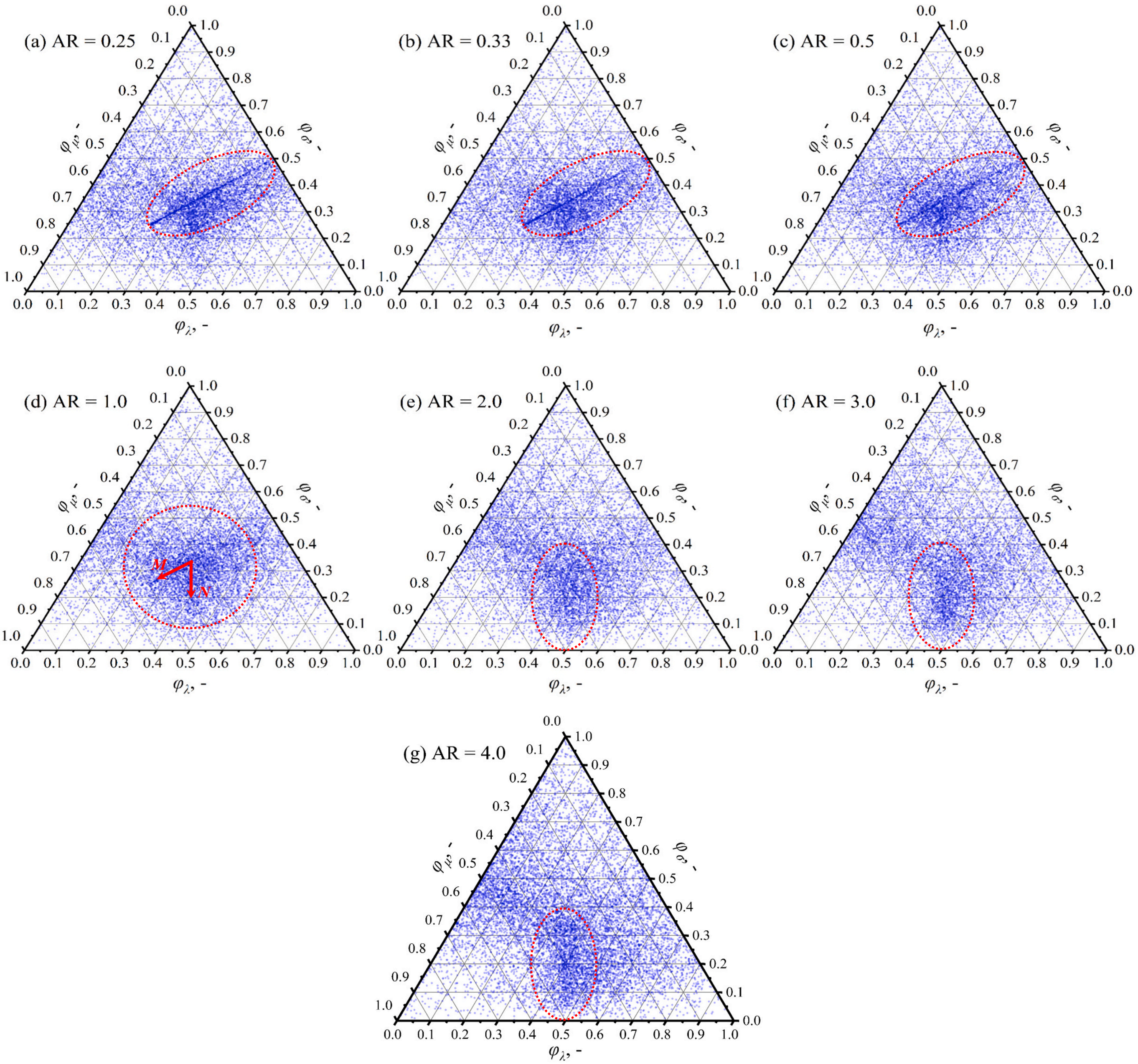

Fig. 7. Influences of AR on the orientation (φ_λ, φ_σ, φ_μ) of cylindrical particles at 45 rpm.

aforementioned preferred mixtures (AR = 1.0 and ω = 45 rpm) are investigated. Here, the mass fraction (φ_c) in this work is controlled by changing the mass ratio of cylindrical particles versus total particles. According to the Eq. 6, Fig. 9 shows that the Lacey mixing index of the mixtures with different φ_c finally reaches a stable value as the drum rotates. In order to quantitatively confirm the effect of φ_c on the mixing process, the inset figure in Fig. 9 shows that the equilibrium mixing index with $\varphi_c = 0.4$ and $\varphi_c = 0.5$ is larger. In addition, the mixture of unitary spheres has a higher mixing rate than that of unitary cylinders. The mixing rate of the mixtures with $\varphi_c > 0.5$ is smaller, and the mixing rate of most mixtures with different φ_c is lower than that of the mixture of unitary cylinders. However, the mixing rate of the mixtures with $\varphi_c < 0.5$ is the opposite, and the mixing rate is better than that of the mixture of unitary spheres. To sum up, the maximum equilibrium mixing index and mixing rate can be achieved when $\varphi_c = 0.4$.

For the behavior that the mixing rate increases initially, followed by a decrease, but then again increases with the increase of φ_c, corresponding mechanisms are necessary to be revealed. For the binary system, the total translational and rotational kinetic energy can be expressed as:

$$E_T(t) = \frac{1}{2}\sum_{i}^{N_i} m_i v_i^2(t) \tag{8}$$

$$E_R(t) = \frac{1}{2}\sum_{i}^{N_i} J_i \omega_i^2(t) \tag{9}$$

For a spherical particle and a cylindrical particle, the average translational and rotational kinetic energy can be expressed as:

$$\overline{E_T}(t) = \frac{1}{2}\sum_{i}^{N_i} m_i v_i^2(t) \Big/ N_i \tag{10}$$

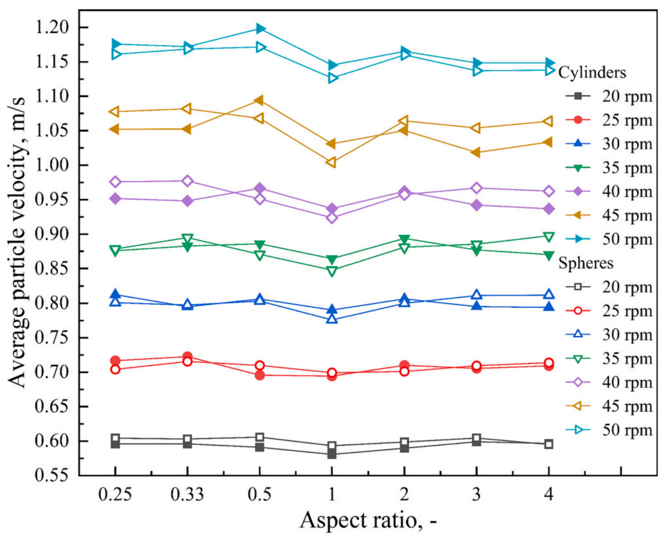

Fig. 8. Evolution of average particle velocity as a function of AR at each ω.

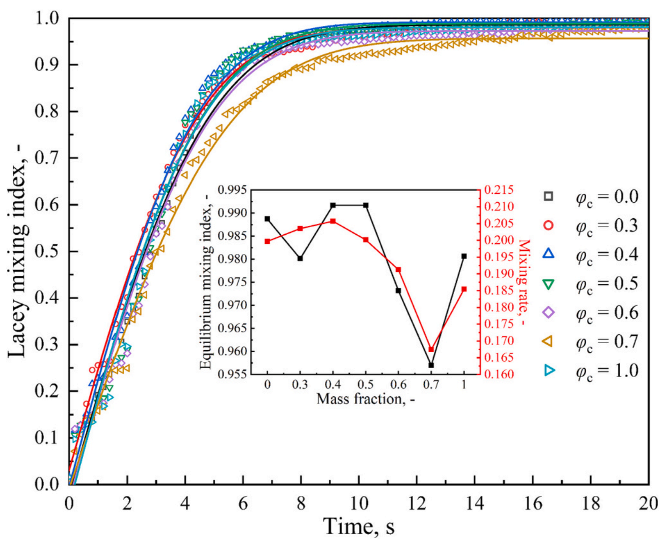

Fig. 9. Evolution of the Lacey mixing index for the aforementioned preferred mixtures (AR = 1.0 and 45 rpm) with time under different φ_c, where the inset figure shows the effect of φ_c on the equilibrium mixing index and the mixing rate.

$$\overline{E_R}(t) = \frac{1}{2}\sum_{i}^{N_i} J_i \omega_i^2(t)/N_i \tag{11}$$

where J_i is the moment of inertia expressed as $J_i = m_i r_i^2$. Fig. 10(a) shows that the translational kinetic energy increases with φ_c followed by cubic polynomial function, and the translational kinetic energy of a cylindrical particle is significantly larger than that of a spherical particle as shown in the inset figure. On the contrary, the rotational kinetic energy decreases with the increase of φ_c in a cubic polynomial function as shown in Fig. 10(b), and the rotational kinetic energy of a spherical particle is significantly higher than that of a cylindrical particle in the inset figure. The relationship between φ_c and the translational/rotational kinetic energy can be divided into three stages. In the first stage, when $\varphi_c < 0.4$, the translational kinetic energy of the mixtures increases obviously and the rotational kinetic energy decreases sharply, which indicates that with the increase of φ_c, the particulate system obtains more energy and has obvious interlocking effect. In this stage, the behavior of more energy input to improve the mixing process is significantly better than that of the interlocking effect to inhibit the mixing process between particles. In the second stage, when φ_c increases from 0.4 to 0.7, the translational kinetic energy of the mixtures increases slightly and the rotational kinetic energy decreases slowly, which increases energy input and reinforces the interlocking effect of the granular system. Meanwhile, the behavior of more energy input to improve the mixing process is weaker than that of the interlocking effect to inhibit the mixing process between particles. The third stage corresponds to $\varphi_c > 0.7$. In this stage, the translational kinetic energy increases obviously and the rotational kinetic energy decreases sharply, which leads to the enhancement of energy input and the interlocking effect of the binary system, respectively. It is worth noting that the behavior of more energy input to improve the mixing process is greater than that of the interlocking effect to inhibit the mixing process. In a word, the mixing process of binary spherical and cylindrical particles with different φ_c is mainly affected by energy input and the interlocking effect.

3.4. The influences of volume fraction on mixing

Besides, we also explore the influence of volume fraction on the mixing process. Here, the volume fraction can be expressed as:

$$\varphi_v = V_c/V_s \tag{12}$$

where V_c, V_s are the volume of a cylindrical particle and a spherical particle, respectively. When V_c is constant (AR = 1.0, d_v = 12 mm) and V_s increases, φ_v is >1.0; when V_s is constant (d_s = 12 mm) and V_c increases, φ_v is <1.0. It can be seen from Fig. 11 that when t = 16 s, the particle system is in a relatively stable state. The inset figure in Fig. 11 shows that the equilibrium mixing index increases and then decreases gradually with φ_v <1.0, which represents an increase and then a decrease gradually in the mixing quality. The equilibrium mixing index decreases sharply with φ_v >1.0, which means a sharp decrease in the mixing quality. In addition, the mixing rate decreases with φ_v away from 1.0, and the mixing rate decreases more obviously when $\varphi_v < 1.0$. In conclusion, the equilibrium mixing index is maximum when $\varphi_v = 0.71$, and the mixing rate is maximum when $\varphi_v = 1.0$.

Therefore, when the binary mixture is in a steady state (t = 16 s), the influence of φ_v on the mixing quality is explained by analyzing the absolute value of the difference (ΔT, ΔR) and the sum (ΣT, ΣR) of the kinetic energy between spherical particles and cylindrical particles. As shown in Fig. 12(a), ΣT increases when $\varphi_v < 1.0$. This is due to the fact that the increase of the volume of spherical particles promotes the binary system to obtain more energy. Interestingly, the case of $\varphi_v > 1.0$ shows the same evolution trend. The difference is that the increase in the volume of cylindrical particles causes the granular system to gain more energy. In addition, ΔT increases with φ_v far away from 1.0. Among them, the case of $\varphi_v > 1.0$ shows a stronger increasing trend. Therefore, it can be inferred that cylindrical particles are more significant in obtaining energy than spherical particles when the volume of spherical or cylindrical particles increases by the same scale. Fig. 12(b) shows that ΣR increases as φ_v is far away from 1.0. This is the reason that the increase in the volume of spherical/cylindrical particles causes the granular system to gain more rotational kinetic energy. Additionally, ΔR gradually decreases with the increase of φ_v. This is because the decrease of the volume of spherical particles dominating the rotational kinetic energy and the increase of the volume of cylindrical particles decreases the difference of the rotational kinetic energy. In summary, with φ_v <0.71, the increase of the volume difference between particles makes the granular bed appear slight segregation behavior, which decreases the mixing quality [59]. When $0.71 < \varphi_v < 1.0$, the decrease of the kinetic energy of granular system makes the convection and diffusion between particles incomplete, but the mixing time is shorter due to the decrease of the volume difference between particles. When $\varphi_v > 1.0$, cylindrical particles dominate the mixing process, and the complex interlocking structure between particles greatly limits the mixing quality.

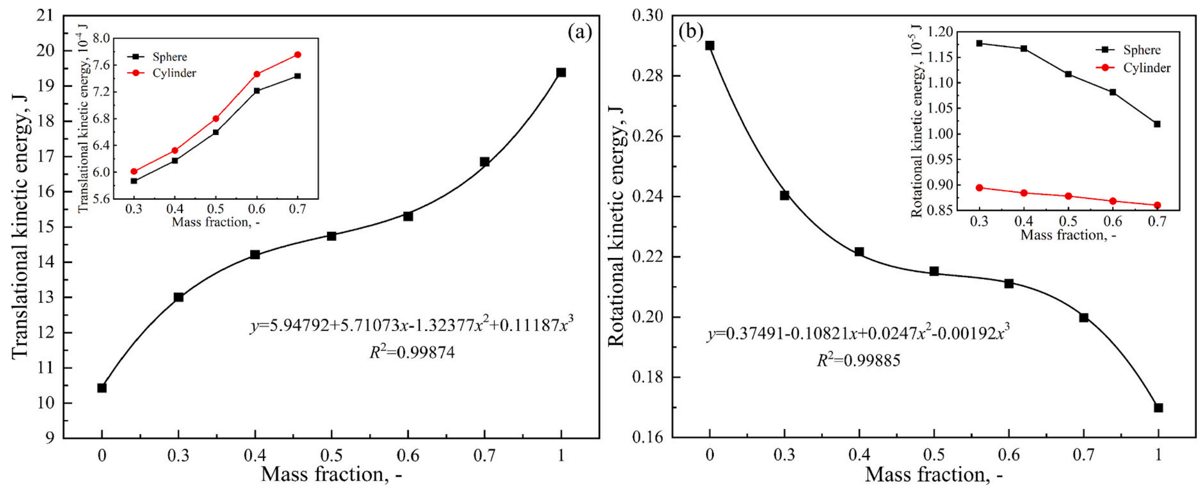

Fig. 10. Total translational (a) and rotational (b) kinetic energy evolution of binary mixtures with different φ_c, where the inset figures show the evolution of average translational and rotational kinetic energy of a spherical particle and a cylindrical particle in binary mixtures with different φ_c.

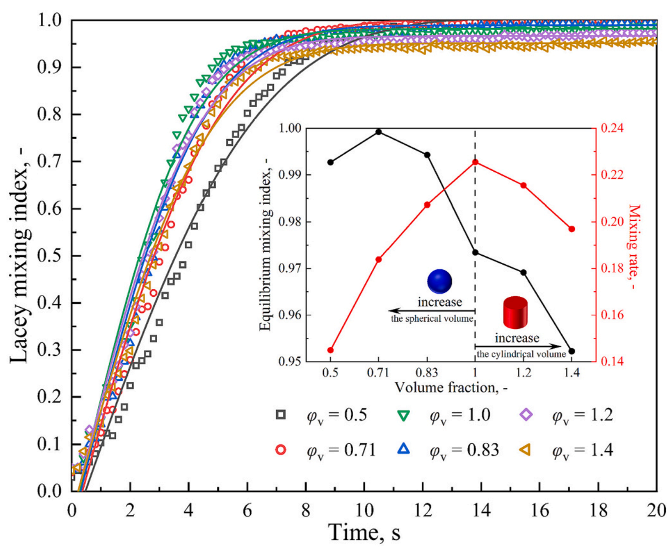

Fig. 11. Evolution of the Lacey mixing index for the aforementioned preferred mixtures (AR = 1.0 and 45 rpm) with time under different φ_v, where the inset figure shows the effect of φ_v on the equilibrium mixing index and the mixing index.

3.5. The influences of density on mixing

As an important material property, the density cannot be omitted during mixing. Therefore, we explored the influence of the density difference ($\varphi_\rho = \rho_s/\rho_c$) on the mixing quality, as shown in Table 2. Here, ρ_s and ρ_c represent the density of spheres and cylinders, respectively. Fig. 13(a) shows that the equilibrium mixing index decreases with the increase of φ_ρ, which indicates that the mixing quality becomes worse. This is because with the increase of φ_ρ, the light particles (cylinders) are closer to the inner walls of the drum and the heavy particles (spheres) are in the center of the granular system, as shown in Fig. 13(b). This limits the diffusion between particles and degrades the mixing quality. This phenomenon is consistent with Hayter et al.'s results [59].

In addition, the influence of φ_ρ on mixing quality is analyzed from the perspective of energy. Fig. 14(a) shows that with the increase of φ_ρ, the number of cylindrical particles (blue) in the local rectangular region increases significantly, which represents an effective increase in the contact area between particles and the walls. This is because compared with the point contact between spherical particles and the walls, the contact modes between cylindrical particles and the walls include the point contact, the line contact and the face contact. For this reason, cylindrical particles have a greater advantage in energy input, but also lead to more energy dissipation [56]. Fig. 14(b) shows that both ΔT and ΣT first increase and then decrease. Curiously, ΔT is maximum when $\varphi_\rho = 3.60$, and ΣT is maximum when $\varphi_\rho = 6.67$. As φ_ρ gradually increases to 3.60, the light cylindrical particles tend to contact with the inner walls of the drum, which leads to a gradual increase in the contact area between them. At this stage, the gradual increase of the contact area makes the proportion of energy dissipation in energy input gradually decrease, so the proportion of kinetic energy of the granular system is larger. When $\varphi_\rho > 3.60$, the situation is opposite. Fig. 14(c) shows that both ΔR and ΣR increase with the φ_ρ. On one hand, the interlocking behavior of spherical particles in the center of the granular bed is greatly weakened; on the other hand, cylindrical particles are more inclined to the outside of the granular bed, and there are more freely moving cylindrical particles in the free layer. In short, the increase of φ_ρ can effectively alleviate the interlocking behavior between particles, but it can also greatly reduce the possibility of convection and diffusion between particles.

4. Conclusions

In this paper, the mixing of binary sphere/cylinder particles in a rotating drum has been numerically studied by DEM. The evolution of the macro- and microscopic properties of binary mixtures and the effects of key influential parameters are investigated. The mechanisms for achieving a better mixing quality have also been explored. The following main conclusions can be drawn.

(1) With the increase of ω, particles can reach a higher position and promote the transformation of the flow regime. When the flow regime is rolling/cascading, the mixing quality can be effectively improved; however, when the flow regime is cataracting, the mixing quality becomes worse.
(2) The normal contact forces are mainly distributed in the middle and tail parts of each granular bed, where the contact of the mixture with AR = 1.0 is more frequent. The major axis of prolate cylinders inclines to be parallel to the rotation direction. The radial direction of oblate cylinders tends to be parallel to the rotation direction. On one hand, the interlock between particles is the weakest when AR = 1.0, which enhances the degree of freedom of particles; on the other hand, the porosity is the smallest when AR = 1.0, which increases the contact time and contact force between particles.
(3) The mixture with φ_c = 0.4 is the optimal solution of granular system affected by energy input and the interlocking effect.

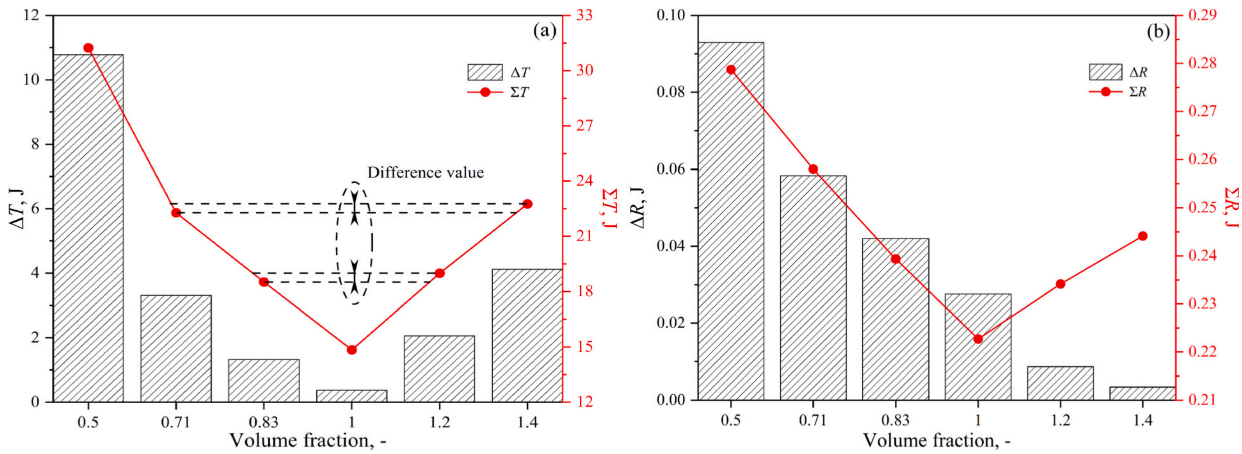

Fig. 12. Evolution of the absolute value of the difference and the sum of translational (a) and rotational (b) kinetic energy between spherical particles and cylindrical particles in binary mixtures with different φ_v.

Table 2
Binary mixtures with different φ_ρ.

Group	1	2	3	4	5
ρ_c, kg/m^3	100	300	500	700	900
ρ_s, kg/m^3	2200	2000	1800	1600	1400
φ_ρ, kg/m^3	22.00	6.67	3.60	2.28	1.56

(4) The larger particles dominate the mixing process, and the volume of spherical particles is more conducive to improving the mixing quality than that of cylindrical particles when the volume of the granular system is at the same level.
(5) With the increase of φ_ρ, the segregation behavior of the spheres and the cylinders occurs. The light particles are closer to the inner walls of the drum and the heavy particles are in the center of the granular bed, which means that the mixing quality becomes worse.

CRediT authorship contribution statement

Chuanning Jiang: Writing – original draft, Methodology, Software, Investigation, Validation, Visualization, Formal analysis. **Xizhong An:** Writing – review & editing, Supervision, Data curation, Formal analysis, Conceptualization, Project administration. **Meng Li:** Writing – review & editing, Supervision, Formal analysis. **Yuhang Wu:** Writing – review & editing, Software, Formal analysis. **Dazhao Gou:** Writing – review & editing, Methodology, Validation. **Yongli Wu:** Writing – review & editing, Visualization.

Declaration of Competing Interest

The authors declare that they have no known competing financial interests or personal relationships that could have appeared to influence the work reported in this paper.

Data availability

Data will be made available on request.

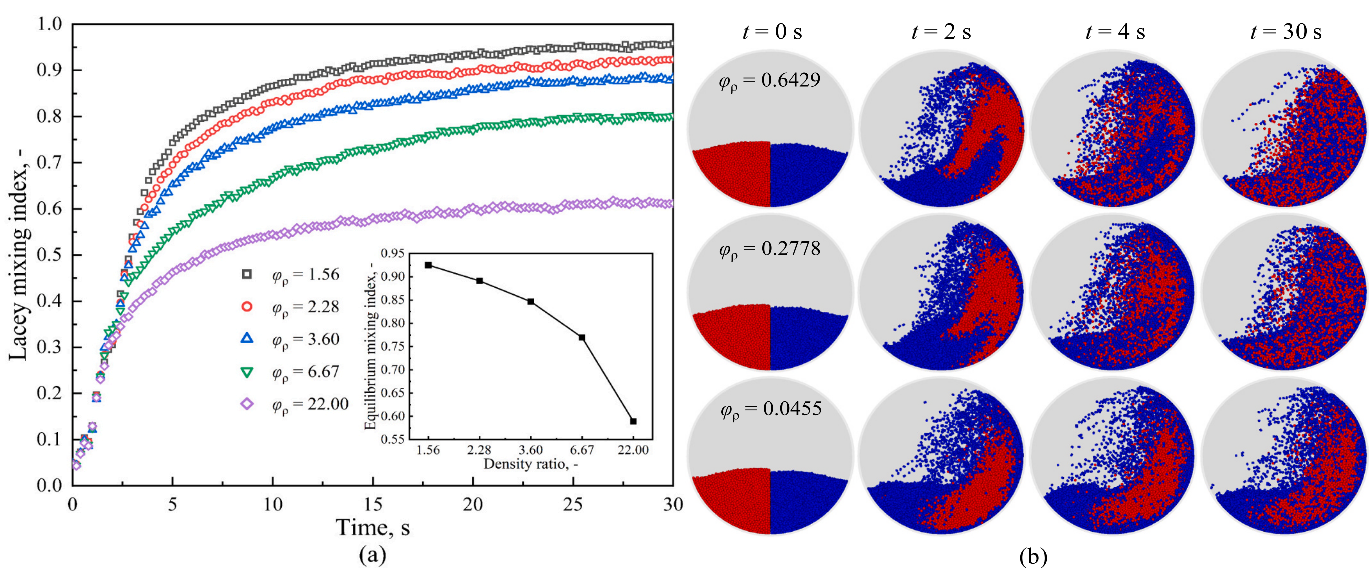

Fig. 13. (a) Evolution of the Lacey mixing index for the aforementioned preferred mixtures (AR = 1.0 and 45 rpm) with time under different φ_ρ, where the inset figure shows the effect of φ_ρ on the equilibrium mixing index; (b) temporal evolution of mixing patterns of spheres (red)/cylinders (blue, AR = 1.0) mixture at different φ_ρ. (For interpretation of the references to colour in this figure legend, the reader is referred to the web version of this article.)

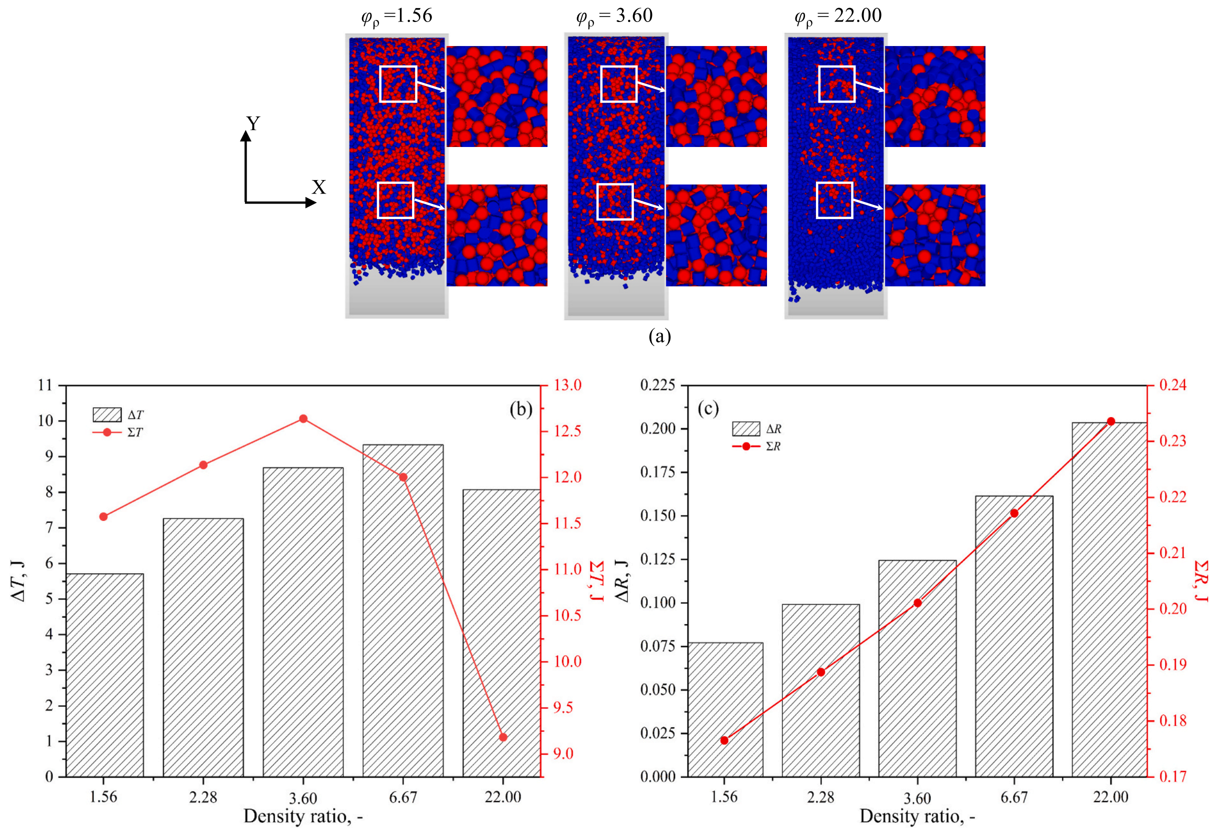

Fig. 14. (a) The process of mixing of the binary mixture at $t = 30$ s at different φ_ρ, where the inset is the zoomed local rectangular region as designated; evolution of the absolute value of the difference and the sum of translational (b) and rotational (c) kinetic energy between spherical particles and cylindrical particles in binary mixtures with different φ_ρ.

Acknowledgments

The authors are grateful to the National Natural Science Foundation of China (No. 51374070) and Liaoning Revitalization Talents Program (XLYC1805007) for the financial support of current work. The authors also acknowledge Prof. Yongzhi Zhao from Zhejiang University for the license provided by DEMSlab Software, which is really a powerful and intelligent platform for particulate researches.

Appendix A. Morphologies of cylindrical particles

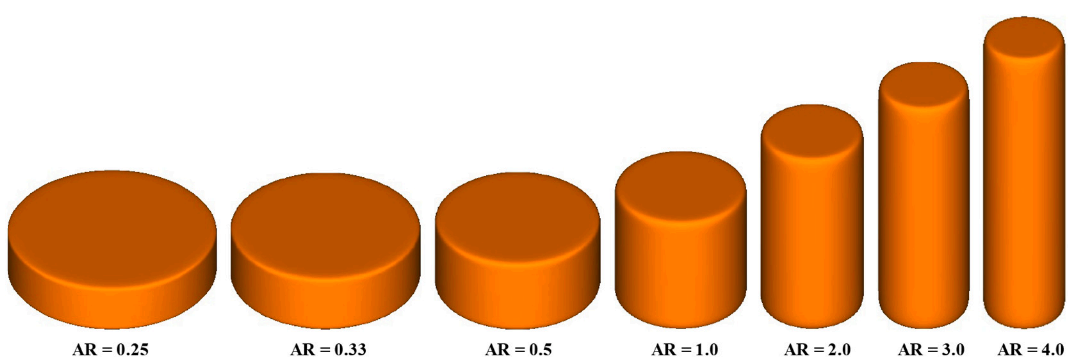

Fig. A1. Cylindrical particles with different ARs used in the simulations.

Appendix B. Model validation

Firstly, the effectiveness of the numerical model was validated by comparing the dynamic slope angles with Maione et al.'s physical experiments of the spheres, cylinders, and the sphere-cylinder mixture ($\varphi_\rho = 7.02$) in the rotating drum under 40 rpm, 20 rpm and 30 rpm, respectively [35], as shown in Fig. A2. In addition, the numerical model is also verified by comparing the concentration of the steel particles obtained from the current work and physical experiments conducted by Maione et al. [35]. One can find that the numerical and experimental results are very comparable, implying the robustness of the established numerical model.

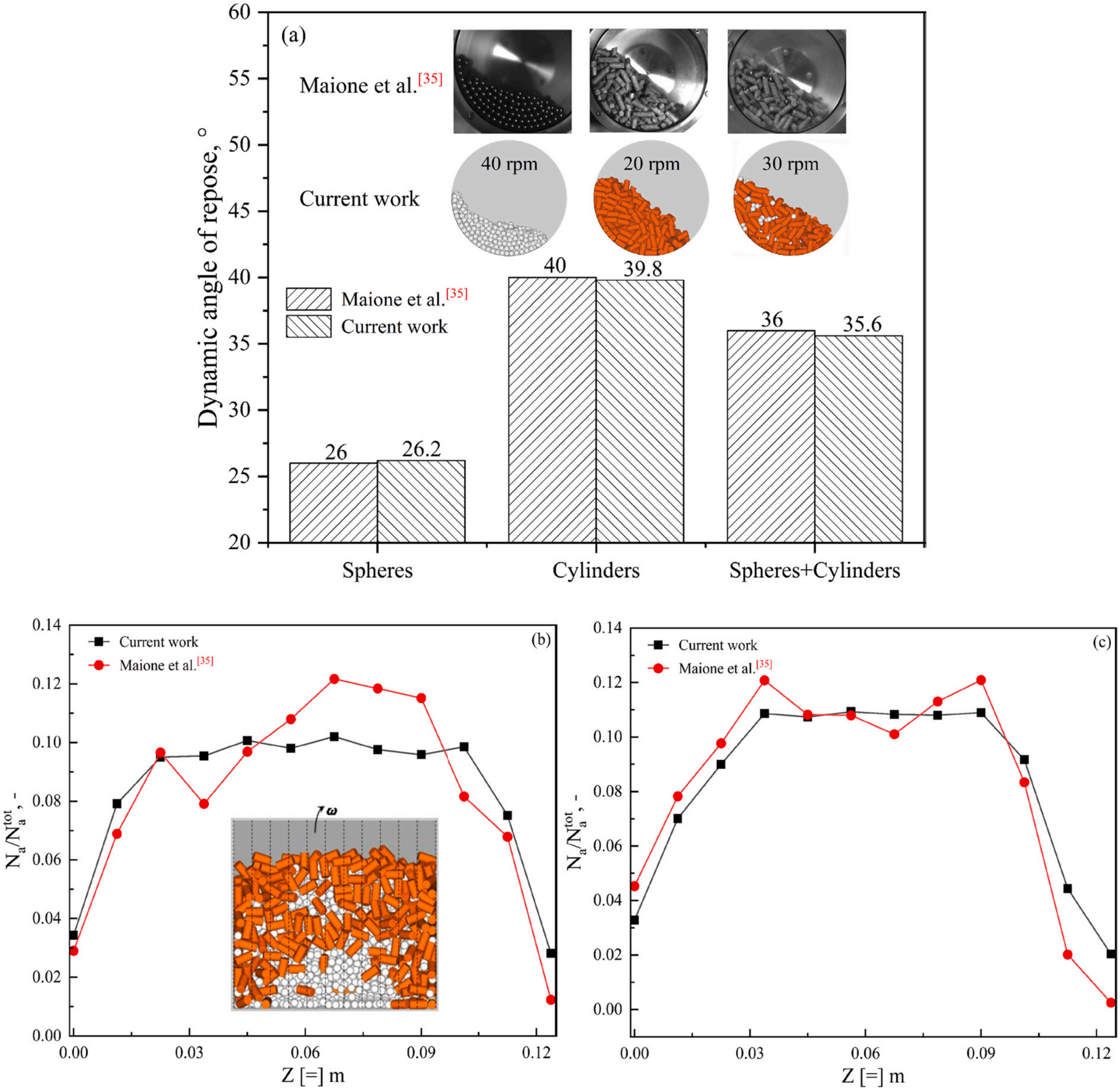

Fig. A2. (a) Comparison of angle of repose between current numerical and Maione et al.'s experimental results for spheres, cylinders, and sphere-cylinder mixture [35]; (b-c) comparison of steel concentration between current work and Maione et al.'s experimental work [35] under different conditions, where the steel concentration is the number of steel particles per axial part divided by the total number of steel particles and the entire system is divided axially into 11 parts.

Appendix C. Mixing index

Here, the Lacey mixing index is defined by:

$$M = \frac{S_0^2 - S^2}{S_0^2 - S_r^2} \tag{A1}$$

where S^2, S_0^2 and S_r^2 are the variance of the current state, the variance in a completely separated state and a completely well-mixed state, respectively, which are given by:

$$S^2 = \frac{1}{k}\sum_{j=1}^{N_S} k_j\left(a_j - \overline{a}\right)^2 \tag{A2}$$

$$S_0{}^2 = P(1-P) \tag{A3}$$

$$S_r{}^2 = \frac{P(1-P)}{n} \tag{A4}$$

where P and (1-P) are the proportions of spherical and cylindrical particles in the binary system; n is the average number of particles in a cell; N_s is the total number of cells in a rotating drum; a_j is the volume ratio of particles of reference type in cell j; $\bar{a}$ is the volume ratio of the referenced particles in a rotating drum; k_j is the weight of cell j and expressed as $k_j = \frac{N_j}{N_t}$ (N_j is the number of particles in cell j, and N_t is the total number of particles); k is the sum of the weights of all cells, described as $k = \sum_{j=1}^{N_s} k_j$.

Appendix D. The evolution of the Lacey mixing index at different conditions

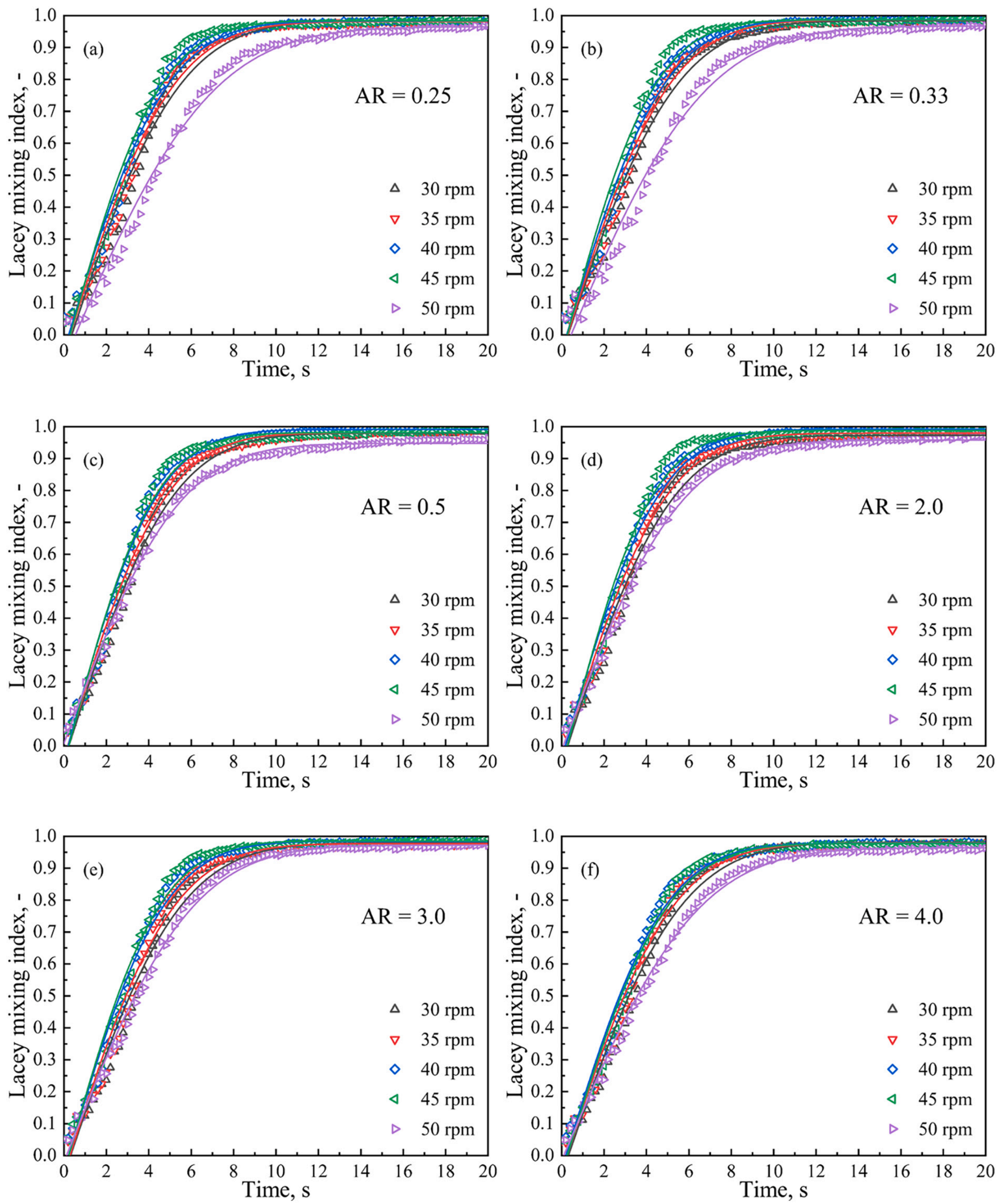

Fig. A3. Lacey mixing index as a function of time at different rotation speeds for the mixtures with AR = 1.0.

References

[1] H. Berthiaux, V. Mosorov, L. Tomczak, C. Gatumel, J.F. Demeyre, Principal component analysis for characterising homogeneity in powder mixing using image processing techniques, Chem. Eng. Process. 45 (2006) 397–403.

[2] J. Mellmann, The transverse motion of solids in rotating cylinders-forms of motion and transition behavior, Powder Technol. 118 (2001) 251–270.

[3] J. Bridgwater, Mixing of powders and granular materials by mechanical means-a perspective, Particuology 10 (2012) 397–427.

[4] M. Nakagawa, S.A. Altobelli, A. Caprihan, E. Fukushima, E. Jeong, Non-invasive measurements of granular flows by magnetic resonance imaging, Exp. Fluids 16 (1993) 54–60.

[5] T.B. Morgan, T.J. Heindel, Sensitivity of X-ray computed tomography measurements of a gas-solid flow to variations in acquisition parameters, Flow Meas. Instrum. 55 (2017) 82–90.

[6] S. Mandal, D.V. Khakhar, An experimental study of the flow of non-spherical grains in a rotating cylinder, AICHE J. 63 (2017) 4307–4315.

[7] M. Rasouli, O. Dubé, F. Bertrand, J. Chaouki, Investigating the dynamics of cylindrical particles in a rotating drum using multiple radioactive particle tracking, AICHE J. 62 (2016) 2622–2634.

[8] T. Finger, F. Von Rüling, S. Lévay, B. Szabó, T. Börzsönyi, R. Stannarius, Segregation of granular mixtures in a spherical tumbler, Phys. Rev. E 93 (2016), 032903.

[9] X. Liu, C. Zhang, J. Zhan, Quantitative comparison of image analysis methods for particle mixing in rotary drums, Powder Technol. 282 (2015) 32–36.

[10] H. Nadeem, T.J. Heindel, Review of noninvasive methods to characterize granular mixing, Powder Technol. 332 (2018) 331–350.

[11] G.G. Pereira, S. Pucilowski, K. Liffman, P.W. Cleary, Streak patterns in binary granular media in a rotating drum, Appl. Math. Model. 35 (2011) 1638–1646.

[12] F. Geng, L. Gang, Y.C. Wang, Y.M. Li, Z.L. Yuan, Numerical investigation on particle mixing in a ball mill, Powder Technol. 292 (2016) 64–73.

[13] H. Chen, Y.G. Xiao, Y.L. Liu, Y.S. Shi, Effect of Young's modulus on DEM results regarding transverse mixing of particles within a rotating drum, Powder Technol. 318 (2017) 507–517.

[14] R.Y. Yang, A.B. Yu, L. McElroy, J. Bao, Numerical simulation of particle dynamics in different flow regimes in a rotating drum, Powder Technol. 188 (2008) 170–177.

[15] W.L. Lo, F.L. Yang, C.S. Chen, S.H. Hsieh, Studying the weak effect of particle friction on the velocity profile of steady dry granular flows in a rotating drum, Granul. Matter 17 (2015) 717–726.

[16] W.J. Rong, Y.Q. Feng, P. Schwarz, T. Yurata, P. Witt, B.K. Li, T. Song, J.W. Zhou, Sensitivity analysis of particle contact parameters for DEM simulation in a rotating drum using response surface methodology, Powder Technol. 362 (2020) 604–614.

[17] N. Gui, J.R. Fan, Numerical simulation of motion of rigid spherical particles in a rotating tumbler with an inner wavelike surface, Powder Technol. 192 (2009) 234–241.

[18] M.Q. Jiang, Y.Z. Zhao, G.S. Liu, J.Y. Zheng, Enhancing mixing of particles by baffles in a rotating drum mixer, Particuology 9 (2011) 270–278.

[19] D. Li, L. Wang, Q. Wang, G.D. Liu, H.L. Lu, Q.H. Zhang, M. Hassan, Simulations of dynamic properties of particles in horizontal rotating ellipsoidal drums, Appl. Math. Model. 40 (2016) 7708–7723.

[20] P.W. Cleary, M.D. Sinnott, Assessing mixing characteristics of particle-mixing and granulation devices, Particuology 6 (2008) 419–444.

[21] G.G. Pereira, P.W. Cleary, De-mixing of binary particle mixtures during unloading of a V-blender, Chem. Eng. Sci. 94 (2013) 93–107.

[22] Y. Xu, C.H. Xu, Z. Zhou, J. Du, D.P. Hu, 2D DEM simulation of particle mixing in rotating drum: a parametric study, Particuology 8 (2010) 141–149.

[23] P.Y. Liu, R.Y. Yang, A.B. Yu, DEM study of the transverse mixing of wet particles in rotating drums, Chem. Eng. Sci. 86 (2013) 99–107.

[24] R.K. Soni, R. Mohanty, S. Mohanty, B.K. Mishra, Numerical analysis of mixing of particles in drum mixers using DEM, Adv. Powder Technol. 27 (2016) 531–540.

[25] N. Gui, X.T. Yang, J.Y. Tu, S.Y. Jiang, Z. Zhang, Numerical simulation of tetrahedral particle mixing and motion in rotating drums, Particuology 39 (2018) 1–11.

[26] C. Wightman, M. Moakher, F.J. Muzzio, O. Walton, Simulation of flow and mixing of particles in a rotating and rocking cylinder, AICHE J. 44 (1998) 1266–1276.

[27] H. Lu, E. Ip, J. Scott, P. Foster, M. Vickers, L.L. Baxter, Effects of particle shape and size on devolatilization of biomass particle, Fuel 89 (2010) 1156–1168.

[28] M. Kodam, R. Bharadwaj, J. Curtis, B. Hancock, C. Wassgren, Cylindrical object contact detection for use in discrete element method simulations, Part II-experimental validation, Chem. Eng. Sci. 65 (2010) 5863–5871.

[29] Y.Z. Zhao, L. Xu, P.B. Umbanhowar, R.M. Lueptow, Discrete element simulation of cylindrical particles using super-ellipsoids, Particuology 46 (2019) 55–56.

[30] H.Q. Ma, Y.Z. Zhao, Investigating the flow of rod-like particles in a horizontal rotating drum using DEM simulation, Granul. Matter 20 (2018) 41.

[31] S.L. Yang, H. Wang, Y.G. Wei, J.H. Hu, J.W. Chew, Flow dynamics of binary mixtures of non-spherical particles in the rolling-regime rotating drum, Powder Technol. 361 (2020) 930–942.

[32] S.L. Yang, Y.H. Sun, J.W. Chew, Simulation of the granular flow of cylindrical particles in the rotating drum, AICHE J. 64 (2018) 3835–3848.

[33] Z.H. Wang, K.D. Wan, J. Xia, Y. He, Y.Z. Liu, J.Z. Liu, Pyrolysis characteristics of coal, biomass, and coal-biomass blends under high heating rate conditions: effects of particle diameter, fuel type, and mixing conditions, Energy Fuel 29 (2015) 5036–5046.

[34] A. Kurniawan, K. Abe, T. Nomura, T. Akiyama, Integrated pyrolysis-tar decomposition over low-grade iron ore for ironmaking applications: effects of coal-biomass fuel blending, Energy Fuel 32 (2018) 396–405.

[35] R. Maione, S.K.D. Richter, G. Mauviel, G. Wild, Axial segregation of a binary mixture in a rotating tumbler with non-spherical particles: experiments and DEM model validation, Powder Technol. 3 (2017) 120–129.

[36] S.Y. Ji, S.Q. Wang, Z.Y. Zhou, Influence of particle shape on mixing rate in rotating drums based on super-quadric DEM simulations, Adv. Powder Technol. 31 (2020) 3540–3550.

[37] M. Li, Y.H. Wu, Y.Q. Qian, X.Z. An, H.Y. Li, DEM simulation on mixing characteristics and macroscopic/microscopic flow behaviors of different-shaped sphero-cylinders in a rotating drum, Ind. Eng. Chem. Res. 60 (2021) 8874–8887.

[38] A.H. Barr, Superquadrics and angle-preserving transformations, IEEE Comput. Graph. Appl. 1 (1981) 11–23.

[39] P.A. Cundall, O.D. Strack, A discrete numerical model for granular assemblies, Géotechnique 29 (1979) 47–65.

[40] G. Lu, J. Third, C. Müller, Discrete element models for non-spherical particle systems: from theoretical developments to applications, Chem. Eng. Sci. 127 (2015) 425–465.

[41] J.Q. Gan, Z.Y. Zhou, A.B. Yu, Particle scale study of heat transfer in packed and fluidized beds of ellipsoidal particles, Chem. Eng. Sci. 144 (2016) 201–215.

[42] T. Stedile, L. Ender, H.F. Meier, E.L. Simionatto, V.R. Wiggers, Comparison between physical properties and chemical composition of bio-oils derived from lignocellulose and triglyceride sources, Renew. Sust. Energ. Rev. 50 (2015) 92–108.

[43] M.N. Acda, Fuel pellets from downed coconut (*cocos nucifera*) in super typhoon Haiyan, Biomass Bioenergy 83 (2015) 539–542.

[44] C.D. Blasi, Influences of physical properties on biomass devolatilization characteristics, Fuel 76 (1997) 957–960.

[45] M.R. Wu, D.L. Schott, G. Lodewijks, Physical properties of solid biomass, Biomass Bioenergy 35 (2011) 2093–2105.

[46] A.A.B. Pécora, I. Ávila, C.S. Lira, G. Cruz, P.M. Crnkovic, Prediction of the combustion process in fluidized bed based on physical-chemical properties of biomass particles and their hydrodynamic behaviors, Fuel Process. Technol. 124 (2014) 188–197.

[47] B. Zhang, C.Y. Zhou, Z.Q. Chen, Y.M. Zhao, Effect of coal particle swarm properties on the fluidization characteristics and coal beneficiation in a dense-phase gas-solid fluidized bed, Particuology 35 (2017) 108–118.

[48] P.S. Dash, S.H. Kriahnan, R. Sharma, P.K. Banerjee, S.K. Haldar, Laboratory scale investigation to improve the productivity of stamp charge coke oven through optimisation of bulk density of coal cake, ISIJ Int. 45 (2005) 1577–1586.

[49] B. Zhang, Y.M. Zhao, Z.F. Luo, S.L. Song, G.M. Li, C. Sheng, Utilizing an air-dense medium fluidized bed dry separating system for preparing a low-ash coal, Int. J. Coal Prep. Util. 34 (2014) 285–295.

[50] M.S.A. Perera, P.G. Ranjith, S.K. Choi, A. Bouazza, J. Kodikara, D. Airey, A review of coal properties pertinent to carbon dioxide sequestration in coal seams: with special reference to Victorian brown coals, environ, Earth Sci. 64 (2011) 223–235.

[51] M. Du, F. Gao, C. Cai, S. Su, Z. Wang, Differences in petrophysical and mechanical properties between low- and middle-rank coal subjected to liquid nitrogen cooling in coalbed methane mining, ASME. J. Energy Resour. Technol. 144 (2022), 042303.

[52] M. Danby, J. Shrimpton, M. Palmer, On the optimal numerical time integration for DEM using Hertzian force models, Comput. Chem. Eng. 58 (2013) 211–222.

[53] S.Y. He, J.Q. Gan, D. Pinson, A.B. Yu, Z.Y. Zhou, Flow regimes of cohesionless ellipsoidal particles in a rotating drum, Powder Technol. 354 (2019) 174–187.

[54] P.M.C. Lacey, Development in the theory of particle mixing, J. Appl. Chem. 4 (1954) 257–268.

[55] S.Y. He, J.Q. Gan, D. Pinson, A.B. Yu, Z.Y. Zhou, A discrete element method study of monodisperse mixing of ellipsoidal particles in a rotating drum, Ind. Eng. Chem. Res. 59 (2020) 12458–12470.

[56] N. Gui, X.T. Yang, J.Y. Tu, S.Y. Jiang, Numerical simulation and analysis of mixing of polygonal particles in 2D rotating drums by SIPHPM method, Powder Technol. 318 (2017) 248–262.

[57] M. Li, X.Z. An, Mixing characteristics and flow behaviors of different shaped tetrahedra in a rotary drum: a numerical study, Powder Technol. 417 (2023), 118262.

[58] R. Hogg, D.W. Fuerstenau, Transverse mixing in rotating cylinders, Powder Technol. 6 (1972) 139–148.

[59] D. Hayter, G. Pereirab, K. Liffman, B. Aldhamc, S. Johnsc, I.D. Sutaloc, G. Brooks, P. Cleary, G. Metcalfe, Density segregation of granular material in a rotating cylindrical tumbler, Proc. SPIE 7270 (2009), 727010.